

STABILITY OF BEAMS SUBJECTED TO
THERMAL IMPERFECTIONS

By

KAH-KAN CHAN

Bachelor of Science

Oklahoma State University

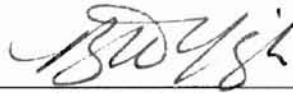
Stillwater, Oklahoma

1997

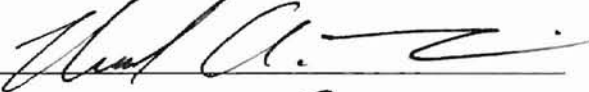
Submitted to the Faculty of the Graduate College
of the Oklahoma State University
in partial fulfillment of the requirements
for the Degree of
MASTER OF SCIENCE
July, 1999

STABILITY OF BEAMS SUBJECTED TO
THERMAL IMPERFECTIONS

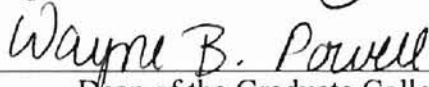
Thesis Approved:



Thesis Adviser



G. Steven Gjirson



Dean of the Graduate College

ACKNOWLEDGMENTS

I sincerely thank my adviser, Dr. Bjong Yeigh. I am indebted to him for his criticism, motivation, and inspiration. His criticism helped me to produce quality research and even more helped me to become a mature engineer. He gave me the opportunity to "learn by doing" and built my confidence by showing me how to tackle difficult problems.

I also thank my thesis committee, Dr. G. Steven Gipson and Dr. Richard A. DeVries. Dr. Gipson did a tremendous job in teaching me the energy method. Dr. DeVries showed me that the design world is full of joy and excitement.

A special thanks goes to my friend and secretary, Charly Fries, who edited this thesis and who was always there when I needed her.

Most importantly, I would like to thank my beloved, Ai-Chin (OSU '98), who struggled through the tough times with me. Without her support and encouragement I would have given up long ago. I am grateful to my parents for their support and encouragement.

The author acknowledges the support from the Center for Sensor Technologies, Dr. James P. Wicksted, Director.

TABLE OF CONTENTS

Chapter	Page
1. INTRODUCTION	1
2. CRITICAL IMPERFECTION MAGNITUDE METHOD	5
3. BEAM ON ELASTIC FOUNDATION	11
4. COMPUTATION METHODS AND RESULTS	20
5. CONCLUSIONS	34
6. REFERENCES	36

LIST OF FIGURES

Figure	Page
1.1. Buckling Response of Imperfection-Insensitive Structure	2
1.2. Buckling Response of Imperfection-Sensitive Structure	3
2.1. Load-Displacement Diagram	8
3.1 Beam on Elastic Foundation	12
4.1 Convergence of Imperfection Modes	25
4.2 Convergence of Buckling Modes	26
4.3 Effects on Foundation Stiffness on ϵ_{RMS}^f	27
4.4 Direct Comparison of e, f, g, h, and t	28
4.5 Effects on change in temperature ϵ_{RMS}^t	29
4.6 Figure 4.6: Effects on Initial Shape ϵ_{RMS}^h and ϵ_{RMS}^l	30
4.7 Effects on Modulus of Elasticity ϵ_{RMS}^e	31
4.8 Effects on Foundation Stiffness ϵ_{RMS}^f	32
4.9 Effects on Moment of Inertia ϵ_{RMS}^i	33

NOMENCLATURE

A	cross-section area
C_t	foundation stiffness factor
E	elastic modulus
E_0	elastic modulus (mean value)
F	foundation stiffness
I	moment of inertia
I_0	moment of inertia (mean value)
L	beam length
L_p	modified beam length
M	number of generalized coordinates
N	number of imperfection modes
P	applied axial load
q	generalized coordinates
r	inverse geometric stiffness matrix
T	change in temperature
T_0	change in temperature (mean value)
V	total potential energy function
v	non-dimensional total potential energy
W	lateral deflection

w	non-dimensional lateral deflection
$w_0(x)$	non-dimensional initial shape deformity
X	axial coordinate
x	non-dimensional axial coordinate
X^*	fixed spatial coordinate
φ	non-dimensional foundation stiffness
φ_0	non-dimensional foundation stiffness (mean value)
a, b, c, d	coefficients of the potential energy expansion
e_j, f_j, g_j, h_j, t_j	amplitude of imperfection pattern
j, k, l, m	mode order subscripts
$e(x)$	elastic modulus imperfection pattern
$f(x)$	foundation stiffness imperfection pattern
$g(x)$	moment of inertia imperfection pattern
$h(x)$	shape imperfection pattern
$t(x)$	change in temperature imperfection pattern
γ	coefficient of the eigenvalue problem
δ_{jk}	Kronecker Delta
δ_q	virtual change in the generalized coordinate q
δV	first variation of the potential energy
δv	non-dimensional first variation of the potential energy

δ^2V	second variation of potential energy
δ^2v	non-dimensional second variation of potential energy
ϵ	universal imperfection magnitude
ϵ_{cr}	critical imperfection magnitude
ϵ_{RMS}	root mean square critical imperfection magnitude
α	coefficient of thermal expansion
ρ	non-dimensional buckling load of the actual structure
ρ_{cl}	non-dimensional classical buckling load of the actual structure

CHAPTER 1

INTRODUCTION

As the integrated circuit (IC) has revolutionized information technology, micro-electromechanical systems (MEMS) have opened up numerous ways to affect our everyday lives. Microengines, microsensors, and micromachines are no larger than the size of a dust particle. MEMS will one day drive the submarine capsule inside our blood vessels to unclog blockages and more. Is this science fiction? The miniaturization revolution has begun.

Microsensors and microengines are not only small but are also fragile. Small imperfections in shape, materials, and operating conditions could severely limit their use. Consequently, one of the many goals for MEMS is increasing their durability. How microsensors behave in less than perfect conditions is of great interest. How will the stability of these microdevices be affected?

Failure analysis based on strength and stiffness or stability is an important and integral component of structural design. Tension failure is dependent on strength and stiffness only, and occurs when normal stress of a member exceeds stress limits (yield or ultimate) of the material. However, failure of a slender compression member is dependent on strength, stiffness, and most critically stability; this member can fail before reaching its stress limits. Material strength consideration alone is not sufficient to predict structural behavior.

Engineers predict critical buckling load of structures by several methods. Two predominant classical stability analyses are differential equations and energy method approaches. In theory these approaches have worked well for conservative structures that are insensitive to imperfections, but in practice no structure has perfect geometry or shape

and the applied load may not be concentric. Tolerances account for irregularities and variabilities in the fabrication and assembly of structural members.

Cylindrical shells and beams on elastic foundations are two structure types that are sensitive to imperfections [Tennyson, Muggeridge, and Caswell 1971; Almroth, Holmes, and Brush 1964]. Bifurcation buckling strength of these structure types is sensitive to the presence of small structural imperfections in material, geometry, and load. Some researchers have defined structural imperfections as any small and unintended deviations or variations from the perfect structure [Palassopoulos 1993, Yeigh 1995]. Timoshenko and Gere [1961] showed that equilibrium of a given structure is stable at the critical load if the structure is insensitive to imperfections. The response of imperfection-insensitive structures is shown in *Figure 1.1*.

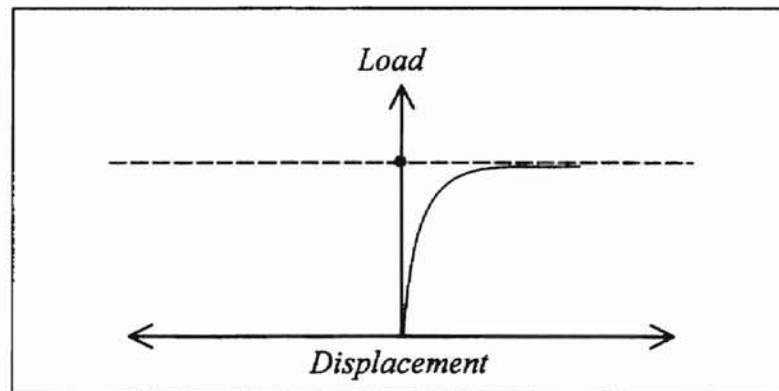


Figure 1.1. Buckling Response of Imperfection-Insensitive Structure

If the structure is sensitive to imperfections, the neighboring equilibrium position exists at loads smaller than the critical load; this equilibrium position is unstable [Simitses 1976]. The critical load of an imperfection-sensitive structure may be considerably smaller than that of an idealized perfect model due to the presence of small imperfections [Simitses 1976]. The load-displacement response of an imperfection-sensitive structure is shown in *Figure 1.2*. The nature of structural imperfections is

generally small and unavoidable. Imperfections considered in this study include variabilities in initial shape, modulus of elasticity, moment of inertia, foundation stiffness, and temperature. The combined effects of these imperfections are also considered in this research.

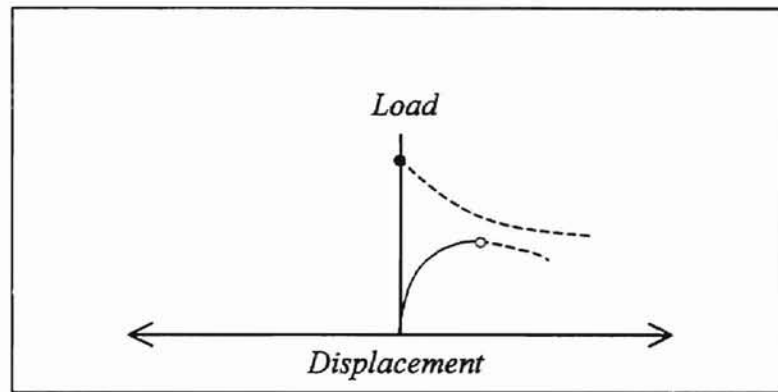


Figure 1.2. Buckling Response of Imperfection-Sensitive Structure

In large structures, engineers frequently use safety factors (SF) to mask structural imperfections. Although a large SF is used to account for uncertainties in the actual structure, such an SF will often produce uneconomic and overdesigned structures and may decrease safety. For example, a structure with excessive stiffness will respond adversely under high-frequency seismic or wind loads.

The most widely used buckling equation was derived by Leonhard Euler to calculate the critical load of a concentrically-loaded column in 1744. Commonly known as the Euler formula, this equation is fundamental for the design and analysis of most buckling problems. Unfortunately, this equation can be used only for perfect elastic columns.

In the past 50 years, much stability research has been based on the classical method. In 1945, Koiter showed that imperfection effects on structures caused differences between theoretical and experimental results [Koiter 1945, Thompson and Hunt 1984]. Koiter also examined the interaction of various buckling modes that occur at the same

load and analyzed imperfection sensitivity of various structures; however, this investigation was limited to shape imperfection only [Yeigh 1995]. Palassopoulos [1992] stated that the analysis in Koiter's method was based on dominance of the classical buckling mode, but this dominance was valid only asymptotically close to the bifurcation buckling load for the perfect structure. For medium and high imperfection-sensitive structures, the buckling load for the perfect structure extends below the bifurcation load by as much as 70%. Palassopoulos concluded that Koiter's analysis was fundamentally inadequate for cases of medium and high imperfection sensitivity.

A breakthrough in stability research by Palassopoulos [1993] proposed the critical imperfection magnitude (CIM) method. His theory was based on the expansion of potential energy without any limitations to shape imperfection. CIM overcame the limitation of Koiter's theory by placing no restrictions on the type of imperfections. Palassopoulos analyzed imperfection effects for modulus of elasticity, moment of inertia, shape and foundation stiffness, and effects for combined imperfections on the same structure.

Imperfections stemming from changes or variabilities in temperature and their effects on beams (applicable for both large- and microstructures) are the focus of this research. Temperature changes cause material expansion and contraction, and a subsequent increase or decrease in thermal strains and stresses. Even a small temperature decrease can cause warping and cracking in thin films, fibers, microelectromechanical systems, and other thin small structures. In this study, structures are assumed to include no change in elastic and thermal expansion coefficients for low heat and small deflection before buckling occurs. A comprehensive literature search revealed no investigation on the effects of thermal imperfection in buckling analysis. This study will focus on stability behavior of beams on elastic foundations due to the presence of thermal imperfection.

CHAPTER 2

CRITICAL IMPERFECTION MAGNITUDE METHOD

The critical imperfection magnitude (CIM) method is used to determine the effects of imperfections on beams. CIM is chosen for this study because of its simplicity, its versatility, and its ability to consider any sources of structural imperfections. Multiple imperfection types can be considered as long as potential energy for the structures can be written; furthermore, CIM has produced good results [Palassopoulos 1993, Yeigh 1995, Hoffman 1996].

Palassopoulos first introduced this regular perturbation expansion method in 1993. CIM is based on the second-order expansion of the potential energy and the fourth-order expansion of a kinematically admissible set of generalized coordinates. For the present nonlinear problem, the second-order expansion of potential energy has given good results for the inextensional beam on elastic foundation (BEF) [Palassopoulos 1993, Yeigh 1995]. The order of expansion can be unlimited but a higher order expansion leads to increased complexity in both analytical and numerical solutions

A "perfect" structure represents those beams with zero imperfections, while "actual" structures contain imperfections of varying degrees. First, the potential energy of the "perfect" structure, V_0 , is expanded in terms of the kinematically admissible set of generalized coordinates q_j , $j = 1, 2, \dots, M$.

$$V_0 = v_0 + a_{0j}q_j + b_{0jk}q_jq_k + c_{0jkl}q_jq_kq_l + d_{0jklm}q_jq_kq_lq_m + \dots \quad (2.1)$$

The subscript, 0, in variables and coefficients denotes a perfect structure. For the "actual" structure its potential energy, V , is expended about V_0 , which is the potential energy for the corresponding "perfect" structure.

$$V = V_0 + \varepsilon V_1 + \varepsilon^2 V_2 + \dots \quad (2.2)$$

$$V_1 = v_1 + a_{1j}q_j + b_{1jk}q_jq_k + c_{1jkl}q_jq_kq_l + d_{1jklm}q_jq_kq_lq_m + \dots \quad (2.3)$$

$$V_2 = v_2 + a_{2j}q_j + b_{2jk}q_jq_k + c_{2jkl}q_jq_kq_l + d_{2jklm}q_jq_kq_lq_m + \dots \quad (2.4)$$

The universal perturbation parameter is denoted by ε , which must be sufficiently small for the convergence of power series expansion of V . The same parameter, ε , is also used in the expansion of the material, load, and geometric parameters. For example, any geometric or material parameters, $S(x)$, can always be expanded about its mean value, S_0 , and an imperfection pattern, $s(x)$, as $S(x) = S_0 [1 + \varepsilon s(x)]$. If there is no imperfection, either ε or $s(x)$ is zero, and the resulting structure is deemed "perfect".

The coefficients $a_{(\cdot)}$, $b_{(\cdot)}$, $c_{(\cdot)}$, and $d_{(\cdot)}$ in *Equations 2.1-2.4* are chosen to be symmetric with respect to permutation of their indices. The application of symmetry helps to increase the computational efficiency for CIM. Substituting *Equations 2.3* and *2.4* into *Equation 2.2* and rearranging the terms, the potential energy is cast in the following form:

$$\begin{aligned} V = & (v_0 + \varepsilon v_1 + \varepsilon^2 v_2 + \dots) \\ & + (a_{0j} + \varepsilon a_{1j} + \varepsilon^2 a_{2j} + \dots)q_j \\ & + (b_{0jk} + \varepsilon b_{1jk} + \varepsilon^2 b_{2jk} + \dots)q_jq_k \\ & + (c_{0jkl} + \varepsilon c_{1jkl} + \varepsilon^2 c_{2jkl} + \dots)q_jq_kq_l \\ & + (d_{0jklm} + \varepsilon d_{1jklm} + \varepsilon^2 d_{2jklm} + \dots)q_jq_kq_lq_m + \dots \end{aligned} \quad (2.5)$$

The first and second variations δV and $\delta^2 V$ of the potential energy yield equilibrium and stability equations [Bazant 1991, Langhaar 1989, Thompson and Hunt 1984]. Coefficients in the variational equations are grouped in terms of the order of their corresponding generalized coordinates:

$$\Delta V = V(q_j + \delta q_j, q_k + \delta q_k) - V(q_j, q_k) \quad (2.6)$$

$$\begin{aligned} \Delta V = & (a_{0j} + \varepsilon a_{1j} + \varepsilon^2 a_{2j} + \dots)(\Delta q_j) \\ & + (b_{0jk} + \varepsilon b_{1jk} + \varepsilon^2 b_{2jk} + \dots)(\Delta(q_jq_k)) \\ & + (c_{0jkl} + \varepsilon c_{1jkl} + \varepsilon^2 c_{2jkl} + \dots)(\Delta(q_jq_kq_l)) \\ & + (d_{0jklm} + \varepsilon d_{1jklm} + \varepsilon^2 d_{2jklm} + \dots)(\Delta(q_jq_kq_lq_m)) \end{aligned} \quad (2.7)$$

where

$$\Delta q_j = (q_j + \delta q_j) - q_j = \delta q_j \quad (2.8)$$

$$\begin{aligned} \Delta(q_j q_k) &= [(q_j + \delta q_j)(q_k + \delta q_k)] - (q_j q_k) \\ &= q_j(\delta q_k) + q_k(\delta q_j) + (\delta q_j)(\delta q_k) \end{aligned} \quad (2.9)$$

$$\begin{aligned} \Delta(q_j q_k q_l) &= [q_j(\delta q_j)][q_k(\delta q_k)][q_l(\delta q_l)] - (q_j q_k q_l) \\ &= q_j q_k(\delta q_l) + q_l q_j(\delta q_k) + q_k q_l(\delta q_j) + q_j(\delta q_k)(\delta q_l) \\ &\quad + q_l(\delta q_j)(\delta q_k) + q_k(\delta q_l)(\delta q_j) + (\delta q_j)(\delta q_k)(\delta q_l) \end{aligned} \quad (2.10)$$

$$\begin{aligned} \Delta(q_j q_k q_l q_m) &= [q_j + (\delta q_j)][q_k + (\delta q_k)][q_l + (\delta q_l)][q_m + (\delta q_m)] - (q_j q_k q_l q_m) \\ &= q_j q_k q_l q_m + q_j q_k q_l(\delta q_m) + q_j q_k q_m(\delta q_l) \\ &\quad + q_j q_k(\delta q_l)(\delta q_m) + q_j q_l q_m(\delta q_k) + q_j q_l(\delta q_k)(\delta q_m) \\ &\quad + q_j q_m(\delta q_k)(\delta q_l) + q_j(\delta q_k)(\delta q_l)(\delta q_m) \\ &\quad + q_k q_l q_m(\delta q_j) + q_k q_l(\delta q_j)(\delta q_m) + q_k q_m(\delta q_j)(\delta q_l) \\ &\quad + q_k(\delta q_j)(\delta q_l)(\delta q_m) + q_l q_m(\delta q_j)(\delta q_k) \\ &\quad + q_l(\delta q_j)(\delta q_k)(\delta q_m) + q_m(\delta q_j)(\delta q_k)(\delta q_l) \\ &\quad + (\delta q_j)(\delta q_k)(\delta q_l)(\delta q_m) - q_j q_k q_l q_m \end{aligned} \quad (2.11)$$

The first and second variation δV and $\delta^2 V$ equations can be formed by combining *Equations 2.6-2.11*:

$$\begin{aligned} \delta V &= \{(a_{0j} + \epsilon a_{1j} + \epsilon^2 a_{2j} + \dots) \\ &\quad + 2 (b_{0jk} + \epsilon b_{1jk} + \epsilon^2 b_{2jk} + \dots) q_k \\ &\quad + 3 (c_{0jkl} + \epsilon c_{1jkl} + \epsilon^2 c_{2jkl} + \dots) q_k q_l \\ &\quad + 4 (d_{0jklm} + \epsilon d_{1jklm} + \epsilon^2 d_{2jklm} + \dots) q_k q_l q_m\} (\delta q_j) \end{aligned} \quad (2.12)$$

$$\begin{aligned} \delta^2 V &= \{2(b_{0jk} + \epsilon b_{1jk} + \epsilon^2 b_{2jk} + \dots) \\ &\quad + 6 (c_{0jkl} + \epsilon c_{1jkl} + \epsilon^2 c_{2jkl} + \dots) q_l \\ &\quad + 12 (d_{0jklm} + \epsilon d_{1jklm} + \epsilon^2 d_{2jklm} + \dots) q_l q_m\} (\delta q_j)(\delta q_k) \end{aligned} \quad (2.13)$$

CIM requires two independent expansions. The first expansion is the potential energy expansion of the "actual" structures in *Equations 2.12 and 2.13*. In the second expansion, the prebuckling equilibrium state q_j of the actual structure is expanded around the prebuckling equilibrium state q_{0j} of the perfect structure:

$$q_j = q_{0j} + \varepsilon q_{1j} + \varepsilon^2 q_{2j} + \dots \quad (2.14)$$

$$q_j q_k = q_{0jk} + \varepsilon q_{1jk} + \varepsilon^2 q_{2jk} + \dots \quad (2.15)$$

$$q_j q_k q_l = q_{0jkl} + \varepsilon q_{1jkl} + \varepsilon^2 q_{2jkl} + \dots \quad (2.16)$$

$$q_j q_k q_l q_m = q_{0jklm} + \varepsilon q_{1jklm} + \varepsilon^2 q_{2jklm} + \dots \quad (2.17)$$

Palassopoulos [1993] noted that the above expansion introduces only a mild effect on the prebuckling response of the "actual" structure if the imperfections are small. Substituting *Equations 2.14-2.17* into *Equations 2.12 and 2.13* produce the prebuckling equilibrium path for the perfect structure, which is indicated by a solid line in *Figure 2.1*. Along the solid line, the structure is stable until the bifurcation point at point B. At this bifurcation point the second variation, $\delta^2 V$, goes from positive definite to positive semidefinite for the first time.

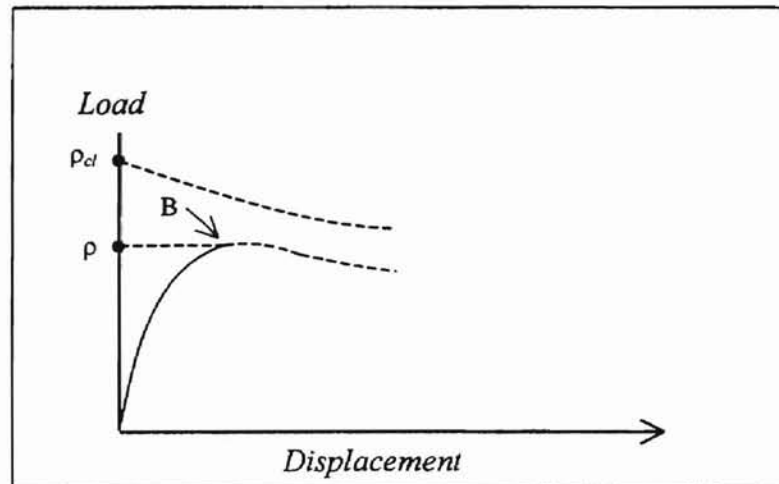


Figure 2.1. Load Displacement Diagram

The traditional approach to solving buckling problems with imperfections is the first to set the level of imperfection at ϵ and then determine the corresponding buckling load. CIM uses an approach that is directly opposite to the traditional one. In CIM the applied load (below buckling load) is forced to determine the level of imperfections necessary to initiate instability. Although CIM may appear to be illogical at first glance, it is actually more logical than the traditional method. The traditional method requires a designer to assume structural imperfections that cannot be determined prior to construction. On the other hand, CIM requires a designer to assume a design load that can be determined after load calculation. Furthermore, CIM provides a guideline for the maximum level of imperfections a structural member can have during the manufacturing or fabrication process. In addition, CIM can be reformulated to work with the traditional approach [Yeigh 1995] where ρ is calculated from the known values of imperfections.

The CIM approach will lead to formulation of a generalized eigenvalue problem in terms of ϵ . There are M eigenvalues in the solution, one for each buckling mode. The smallest eigenvalue is termed the critical imperfection magnitude, ϵ_{cr} , which is the smallest imperfection magnitude permissible prior to bifurcation.

The computation efficiency for the critical imperfection magnitude method can be improved by using incremental coordinates and orthogonal displacement modes. First, the potential energy can be simplified by letting the generalized coordinates be measured incrementally from a reference state of the corresponding perfect structure, $q_j^* = q_j - q_{0j}$, where q_{0j} ($j = 1, 2, \dots, M$) is the prebuckling equilibrium state of the perfect structure. A reference coordinate, q_{0j} , is set to zero, measured from this new reference point; the potential energy expansion can be cast in the following form:

$$(V_{0jk} + \epsilon V_{1jk} + \epsilon^2 V_{2jk} + \dots)(\delta q_k) = 0 \quad (2.18)$$

$$V_{0jk} = 2b_{0jk} \quad (2.19)$$

$$V_{1jk} = 2b_{1jk} + 6c_{0jkl}q_{l1} \quad (2.20)$$

$$V_{2jk} = 2b_{2jk} + 6c_{0jkl}q_{l2} + 6c_{1jkl}q_{l1} + 12d_{0jklm}q_{l1}q_{m1} \quad (2.21)$$

Although it is not required, the coefficients $a_{(\cdot)}$, $b_{(\cdot)}$, $c_{(\cdot)}$, and $d_{(\cdot)}$ are transformed symmetrically with respect to any permutation of their indices ($b_{jk} = b_{kj}$, $c_{jkl} = c_{jlk} = c_{kjl} = c_{klj}$, etc.). The geometric stiffness matrix of the perfect structure, b_{0jk} , in *Equation 2.1* is always positive definite up to the classical buckling load and for the prebuckling range of the imperfection-sensitive structure. The inverse, r_{jk} , always exists ($r_{jk}b_{0jk} = \delta_{jk}$), where δ_{jk} denotes Kronecker's delta ($\delta_{ji} = 1$, $\delta_{jk} = 0$ if $j \neq k$) for the stiffness matrix. Through r_{jk} , the stiffness matrix b_{0jk} can be diagonalized. The transformed generalized coordinates become $q_j^* = r_{jl}q_l^{**}$. These new generalized coordinates— q_j^{**} , $j = 1, 2, \dots, M$, where M represents the number of buckling modes—will produce a Hermitian form of the eigenvalue problem. The new eigenvalue equation is presented as:

$$(\varepsilon\gamma_{1jk} + \varepsilon^2\gamma_{2jk} + \dots)(\delta q_k) = (\delta q_j) \quad (2.22)$$

$$\gamma_{1jk} = \frac{1}{\sqrt{b_{0ij}b_{0kk}}} \left[-b_{1jk} + \frac{3c_{0jkl}a_{1l}}{2b_{0ll}} \right] \quad (2.23)$$

$$\begin{aligned} \gamma_{2jk} = \frac{1}{\sqrt{b_{0ij}b_{0kk}}} \left[-b_{2jk} + \frac{3c_{1jkl}a_{1l}}{2b_{0ll}} + \frac{3c_{0jkl}a_{2l}}{2b_{0ll}} - \frac{3c_{0jkl}b_{1lm}a_{1m}}{2b_{0ll}b_{0mm}} \right. \\ \left. + \frac{9c_{0jkl}c_{0lmn}a_{1m}a_{1n}}{8b_{0ll}b_{0mm}b_{0nn}} - \frac{3d_{0jklm}a_{1l}a_{1m}}{2b_{0ll}b_{0mm}} \right] \end{aligned} \quad (2.24)$$

Further simplification of potential energy can be achieved by using orthogonal-displacement modes. *Equation 2.22* is the general form of the generalized eigenvalue problem, which includes symmetric and asymmetric bifurcation problems. For symmetric bifurcation problems, the third-order coefficient, c_{0jkl} , vanishes identically to zero.

The matrix equivalent for *Equation 2.22* is written as the following:

$$\begin{bmatrix} \gamma_1 & \gamma_2 \\ I & 0 \end{bmatrix} \begin{Bmatrix} \delta q \\ \varepsilon \delta q \end{Bmatrix} = \frac{1}{\varepsilon} \begin{Bmatrix} \delta q \\ \varepsilon \delta q \end{Bmatrix} \quad (2.25)$$

where I and 0 represent identity and zero submatrices. If γ_2 is zero, the resulting eigenvalue problem reduces to $M \times M$. A full solution requires a $2M \times 2M$ eigenvalue problem.

CHAPTER 3

BEAM ON ELASTIC FOUNDATION

A simple model, beam on elastic foundation (BEF), is often used to describe spread footings, grade beams, highway pavements, bridge piers, and sheet pilings. (Note: Some modifications must be made in this research for use in soil foundation problems.) Imperfection sensitivity of BEF can also be extended to describe even the smallest of known structures such as microsensors and microbeams. In this study, BEF is chosen for several reasons. First, the model is simple yet sensitive enough to demonstrate the effects of smallest imperfections. The model has also been examined thoroughly in both deterministic and stochastic analyses. Consequently, much is known about the prototypical model. Finally, the model problem exhibits features readily found in many microdevices such as sensors and actuators on various fixtures and supports.

Five independent imperfections will be considered herein, namely variabilities in initial shape, modulus of elasticity, foundation stiffness, moment of inertia, and temperature.

Consider a simply supported beam on elastic foundation in *Figure 3-1*. The beam is oriented in the standard right-hand system with the positive X-axis pointing to the right, the positive Y-axis pointing down. The beam has length (L), applied load (P), modulus of elasticity (E), moment of inertia (I), and elastic foundation stiffness (F). The temperature change is denoted by T , and the change exerts thermal loads on the beam. Applied loads cause the beam to deflect in the lateral direction; this deflection is represented by W .

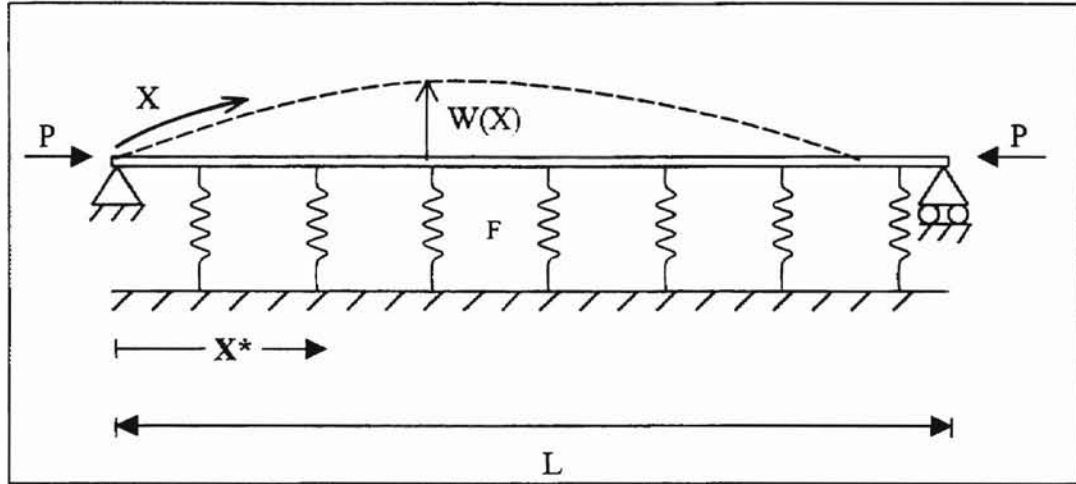


Figure 3.1. Beam on Elastic Foundation

For convenience, dimensional variables have been transformed to dimensionless coordinates. Lengths have been normalized by the modified span length, $L_p = L / \pi$. Other variables such as φ and V have been normalized by their corresponding base values.

$$x = \frac{X}{L_p} = \frac{\pi X}{L} \quad (3.1)$$

$$w = \frac{W}{L_p} = \frac{\pi W}{L} \quad (3.2)$$

$$\varphi = \frac{L_p^4}{E_0 I_0} F = \frac{L^4}{\pi^4 E_0 I_0} F \quad (3.3)$$

$$\rho = \frac{L_p^2}{E_0 I_0} P = \frac{L^2}{\pi^2 E_0 I_0} P \quad (3.4)$$

$$v = \frac{L_p}{E_0 I_0} V = \frac{L}{\pi E_0 I_0} V \quad (3.5)$$

Imperfections also fluctuate about their base values. Such a reference value is the mean value. Shape imperfections deviate from the zero mean since the perfect beam is

straight and rests on the zero-axis. Unlike Type I (shape) imperfections, Type II imperfections fluctuate about some value other than zero. Mean values for Type II imperfections are determined by physical and geometric properties. Mathematically, imperfections can be expressed in the following equations:

$$E(x) = E_0[1 + \epsilon e(x)] \quad (3.6)$$

$$I(x) = I_0[1 + \epsilon g(x)] \quad (3.7)$$

$$\varphi(x) = \varphi_0[1 + \epsilon f(x) + \epsilon C_1 T_0 t(x)] \quad (3.8)$$

$$w_0 = \epsilon h(x) \quad (3.9)$$

$$\varphi_0 = \frac{L_p^4}{E_0 I_0} F_0 = \frac{L^4}{\pi^4 E_0 I_0} F_0 \quad (3.10)$$

$$E(x)A(x) = \frac{E(x)I(x)}{L^2} = \frac{E_0 I_0 [1 + \epsilon e(x)][1 + \epsilon g(x)]}{L^2} \quad (3.11)$$

$$T(x) = T_0[1 + \epsilon t(x)] \quad (3.12)$$

In *Equations 3.6-3.12*, $E(x)$, $I(x)$, $\varphi(x)$, $A(x)$, and $T(x)$ represent elastic modulus, moment of inertia, foundation stiffness, cross section area, and temperature, respectively. Within the imperfection expressions, lowercase letters $e(x)$, $g(x)$, $f(x)$, and $t(x)$ represent deterministic imperfection patterns in elastic modulus, moment of inertia, foundation stiffness, and temperature change; mean values are represented by variables with zero subscripts.

The expression has three components: strain energy, V_B , results from curvature change; potential energy for the applied load and temperature gradient is contained in V_P ; the elastic foundation provides support in the lateral direction and its energy is contained in V_F :

$$V = V_B + V_F + V_P \quad (3.13)$$

$$V_B = \frac{1}{2} \int_0^L EI W''(X^*)^2 dX = \frac{1}{2} \int_0^L EI \left(\frac{W''}{\sqrt{1 - W'^2}} \right)^2 dX \quad (3.14)$$

$$V_F = \frac{1}{2} \int_0^L F W^2 dX \quad (3.15)$$

$$V_P = -(P + P_T) \Delta L = - \left(P - \int_0^L EA \alpha T dx \right) \left(L - \int_0^L \sqrt{1 - W'^2} dX \right) \quad (3.16)$$

where first and second derivatives are denoted by single and double primes. The quantity, X^* , denotes the fixed spatial coordinate which remains in the horizontal direction after the beam bend. Dividing *Equation 3.13* and its components by $(\pi E_0 I_0 / L)$ yield the dimensionless form of the potential energy. For the normalized beam, all integrals are evaluated for $x \in [0, \pi]$:

$$v_B = \frac{1}{2} \int_0^\pi (1 + \varepsilon e)(1 + \varepsilon g) \left[\frac{w''}{\sqrt{1 - w'^2}} - \frac{\varepsilon h''}{\sqrt{1 - \varepsilon^2 h'^2}} \right]^2 dx \quad (3.17)$$

$$v_F = \frac{1}{2} \int_0^\pi \phi_0 (1 + \varepsilon f + \varepsilon C_r T_0 t) (w - \varepsilon h)^2 dx \quad (3.18)$$

$$\begin{aligned} v_P = & -\rho \left(\pi - \int_0^\pi \sqrt{1 - w'^2} dx \right) \\ & - \frac{1}{\pi^2} \left(\int_0^\pi (1 + \varepsilon e)(1 + \varepsilon g)(1 + \varepsilon t) \alpha T_0 dx \right) \left(\int_0^\pi \sqrt{1 - w'^2} dx \right) \\ & + \frac{1}{\pi} \left(\int_0^\pi (1 + \varepsilon e)(1 + \varepsilon g)(1 + \varepsilon t) \alpha T_0 dx \right) \end{aligned} \quad (3.19)$$

Displacements and their derivatives are expanded in Taylor series that are shown in *Equations 3.20-3.21* and substituted into *Equations 3.17-3.19*. Since the CIM method is based on fourth-order expansion of the generalized coordinates, displacements and their fourth-order derivatives of are collected and rearranged:

$$\sqrt{1 - w'^2} = 1 - \frac{1}{2} w'^2 - \frac{1}{8} w'^4 - \frac{1}{16} w'^6 + O(w'^8) \quad (3.20)$$

$$\frac{1}{\sqrt{1-w'^2}} = 1 + \frac{1}{2}w'^2 + \frac{3}{8}w'^4 + \frac{5}{8}w'^6 + O(w'^8) \quad (3.21)$$

$$\begin{aligned} v_B = \frac{1}{2} \int_0^\pi & [(h''^2 - 2(e+g)h''w'' - (e+g)h''w''w'^2 + eg(w'')^2 + eg(w'')^2(w')^2)\epsilon^2 \\ & + (-2h''w'' - h''w''w'^2 + (e+g)(w'')^2 + (e+g)(w'')^2(w')^2)\epsilon \\ & + (w''^2 + w''^2w'^2)] dx \end{aligned} \quad (3.22)$$

$$\begin{aligned} v_f = \frac{1}{2} \int_0^\pi & [(\varphi_0 h^2 - 2\varphi_0(f + C_1 T_0 t)hw)\epsilon^2 - (+2\varphi_0 hw - (f + C_1 T_0 t)\varphi_0 w^2)\epsilon \\ & + (\varphi_0 w^2)] dx \end{aligned} \quad (3.23)$$

$$\begin{aligned} v_p = & -(\rho\pi - \alpha T_0) + \left(\rho - \frac{\alpha T_0}{\pi}\right) \int_0^\pi \left(1 - \frac{1}{2}w'^2 - \frac{1}{8}w'^4\right) dx \\ & + \epsilon \left[\left(\frac{-\alpha T_0}{\pi^2}\right) \int_0^\pi (e+t+g) dx \int_0^\pi \left(1 - \frac{1}{2}w'^2 - \frac{1}{8}w'^4\right) dx + \left(\frac{\alpha T_0}{\pi}\right) \int_0^\pi (e+t+g) dx \right] \\ & + \epsilon^2 \left(\frac{-\alpha T_0}{\pi^2}\right) \int_0^\pi (et+gt+eg) dx \int_0^\pi \left(1 - \frac{1}{2}w'^2 - \frac{1}{8}w'^4\right) dx \\ & + \epsilon^2 \left(\frac{\alpha T_0}{\pi}\right) \int_0^\pi (et+gt+eg) dx \end{aligned} \quad (3.24)$$

Terms in the dimensionless potential energy are grouped into ϵ^a and w^b , and expressed as $v_{a,b}$.

$$v_{0,0} = 0 \quad (3.25)$$

$$v_{0,1} = 0 \quad (3.26)$$

$$v_{0,2} = \int_0^\pi \left[\frac{1}{2}w''^2 + \frac{1}{2}\varphi_0 w^2 - \left(\frac{1}{2}\rho - \frac{\alpha T_0}{2\pi}\right)w'^2 \right] dx \quad (3.27)$$

$$v_{0,3} = 0 \quad (3.28)$$

$$v_{0,4} = \int_0^\pi \left[\frac{1}{2} w''^2 w'^2 - \left(\frac{1}{8} \rho - \frac{\alpha T_0}{8\pi} \right) w'^4 \right] dx \quad (3.29)$$

$$v_{1,1} = \varepsilon \int_0^\pi [-h'' w'' - \varphi_0 h w] dx \quad (3.30)$$

$$v_{1,2} = \varepsilon \int_0^\pi \left(\frac{1}{2} (e+g) w''^2 + \frac{1}{2} \varphi_0 w^2 (f + C_t T_0 t) \right) dx \\ + \varepsilon \left(\frac{\alpha T_0}{\pi^2} \right) \left(\int_0^\pi (e+t+g) dx \right) \left(\int_0^\pi \frac{(w')^2}{2} dx \right) \quad (3.31)$$

$$v_{1,3} = \varepsilon \int_0^\pi \left(-\frac{1}{2} h'' w'' w'^2 \right) dx \quad (3.32)$$

$$v_{2,1} = \varepsilon^2 \int_0^\pi [- (e+g) h'' w'' - \varphi_0 h w (f + C_t T_0 t)] dx \quad (3.33)$$

$$v_{2,2} = \varepsilon^2 \left(\frac{\alpha T_0}{\pi^2} \right) \left(\int_0^\pi (et + gt + eg) dx \right) \left(\int_0^\pi \frac{(w')^2}{2} dx \right) \\ + \varepsilon^2 \left(\int_0^\pi \frac{eg (w'')^2}{2} dx \right) \quad (3.34)$$

It was noted in Chapter 2 that c_{ojkl} vanishes identically to zero for symmetric bifurcation problems. The third-order coefficient in $v_{0,3}$ also vanishes, which verifies that the BEF is indeed a symmetric bifurcation problem.

Before proceeding to the development of the coefficients of $a_{(.)}$, $b_{(.)}$, $c_{(.)}$, and $d_{(.)}$, the potential energy and imperfection patterns should be appropriately discretized. Since the modulus of elasticity, foundation stiffness, moment of inertia, and change in temperature imperfections have no forced boundary conditions, a cosine series can be used to simulate imperfection patterns:

$$e(x) = \sum_{j=1}^N e_j \cos(jx) \quad (3.35)$$

$$g(x) = \sum_{j=1}^N g_j \cos(jx) \quad (3.36)$$

$$f(x) = \sum_{j=1}^N f_j \cos(jx) \quad (3.37)$$

$$t(x) = \sum_{j=1}^N t_j \cos(jx) \quad (3.38)$$

Shape imperfections, on the other hand, are forced to be zero at the boundaries. Consequently, a sine series appears to be more appropriate. The following is the shape imperfection field:

$$h(x) = \sum_{j=1}^N h_j \sin(jx) \quad (3.39)$$

In *Equations 3.35-3.39*, e_j , g_j , f_j , t_j , and h_j are the deterministic imperfection amplitudes and N is the number of imperfection modes which are taken into account in the numerical computations. Similar to shape imperfections, lateral displacement modes are expanded in a sine series to meet the boundary conditions:

$$w(x) = \sum_{j=1}^M q_j \sin(jx) \quad (3.40)$$

where M is the number of displacement modes in the discretized computation.

Substituting imperfection patterns described in *Equations 3.35-3.40* into *Equations 3.25-3.34* and removing the displacements, δq_j , coefficients $a_{(\cdot)}$, $b_{(\cdot)}$, $c_{(\cdot)}$, and $d_{(\cdot)}$ for the generalized eigenvalue problem are obtained:

$$b_{0jk} = \frac{\pi}{4} \left[j^4 - \left(\rho - \frac{\alpha T_0}{\pi} \right) j^2 + \varphi \right] \quad (3.41)$$

$$d_{0jklm} = - \left(\frac{1}{8} \rho - \frac{\alpha T_0}{8\pi} \right) jklm Y_{ijklm} + \frac{1}{12} jklm \left(jk Y_{2jklm} + jl Y_{2jklm} + jm Y_{2jklm} \right. \\ \left. + kl Y_{2kljm} + km Y_{2kmjl} + lm Y_{2lmjk} \right) \quad (3.42)$$

$$a_{ij} = -\frac{\pi}{2}(j^4 + \varphi_0)h_j \quad (3.43)$$

$$b_{1jk} = \frac{1}{2} \sum_{l=1}^N (\varphi_0(f_l + \varphi_0 C_l T_0 t) + j^2 k^2 (e + 4g)) Y_{3jkl} \quad (3.44)$$

$$c_{1jkl} = -\frac{\pi}{6} \sum_{m=1}^N h_m m^2 jkl (j Y_{2mjkl} + k Y_{2mklj} + l Y_{2mjlk}) \quad (3.45)$$

$$b_{2jk} = 2j^2 k^2 e_l g_m Y_{2jklm} + \frac{1}{2} \left(\frac{\alpha T_0}{\pi^2} \right) jk (Y_{3jk})^2 (e_j t_k + 4g_j t_k + 4e_j g_k) \quad (3.46)$$

where

$$Y_{1jklm} = \int_0^{\pi} \cos(jx) \cos(kx) \cos(lx) \cos(mx) dx = \frac{1}{8} \left[\frac{\sin(j-k+l+m)\pi}{j-k+l+m} + \frac{\sin(j-k+l-m)\pi}{j-k+l-m} + \frac{\sin(j-k-l+m)\pi}{j-k-l+m} + \frac{\sin(j-k-l-m)\pi}{j-k-l-m} + \frac{\sin(j+k+l+m)\pi}{j+k+l+m} + \frac{\sin(j+k+l-m)\pi}{j+k+l-m} + \frac{\sin(j+k-l+m)\pi}{j+k-l+m} + \frac{\sin(j+k-l-m)\pi}{j+k-l-m} \right] \quad (3.47)$$

$$Y_{2jklm} = \int_0^{\pi} \sin(jx) \sin(kx) \cos(lx) \cos(mx) dx = \frac{1}{8} \left[\frac{\sin(j-k+l+m)\pi}{j-k+l+m} + \frac{\sin(j-k+l-m)\pi}{j-k+l-m} + \frac{\sin(j-k-l+m)\pi}{j-k-l+m} + \frac{\sin(j-k-l-m)\pi}{j-k-l-m} - \frac{\sin(j+k+l+m)\pi}{j+k+l+m} - \frac{\sin(j+k+l-m)\pi}{j+k+l-m} - \frac{\sin(j+k-l+m)\pi}{j+k-l+m} - \frac{\sin(j+k-l-m)\pi}{j+k-l-m} \right] \quad (3.48)$$

$$\begin{aligned}
Y_{3jkl} &= \int_0^{\pi} \sin(jx) \sin(kx) \cos(lx) dx \\
&= \frac{1}{4} \left[\frac{\sin(j-k-l)\pi}{j-k-l} + \frac{\sin(j-k+l)\pi}{j+k+l} \right. \\
&\quad \left. - \frac{\sin(j+k-l)\pi}{j+k-l} - \frac{\sin(j+k+l)\pi}{j+k+l} \right] \tag{3.49}
\end{aligned}$$

$$\begin{aligned}
Y_{3jk} &= \int_0^{\pi} \cos(jx) \cos(kx) dx \\
&= \frac{1}{2} \left[\frac{\sin(j-k)\pi}{j-k} + \frac{\sin(j+k)\pi}{j+k} \right] \tag{3.50}
\end{aligned}$$

As mentioned in Chapter 2, all variables are now dimensionless. In *Equations 3.47-3.50*, the closed-form expressions for integrals take the following:

$$\lim_{\alpha \rightarrow 0} \frac{\sin \pi\alpha}{\alpha} = \pi \text{ or } \lim_{\alpha \rightarrow 0} \frac{\cos \pi\alpha - 1}{\alpha} = 0 .$$

CHAPTER 4

COMPUTATION METHODS AND RESULTS

A numerical solution of the nonlinear eigenvalue problem discussed in Chapter 2 is time-consuming. This complication stems from a full coefficient matrix, which can be as large as $2M$ by $2M$, where M is the number of buckling modes. Some modifications have been made to the eigenvalue problem to allow a more efficient computation. First, the generalized coordinates have been forced to be measured from the same reference states of the perfect structure. The coefficient matrix was transformed to a symmetric matrix and was then diagonalized. Although these modifications were not necessary for the solution, they optimized the solution process.

A deterministic eigenvalue solver for CIM [Yeigh 1995] was modified to include thermal imperfections. The base program, STABIL1, includes imperfections in shape, foundation stiffness, moment of inertia, and elastic modulus. As a Type II imperfection, temperature variability was modeled with a cosine function. Imperfection patterns in thermal instability were prescribed a priori as were all other imperfection patterns examined in this study.

As described earlier, the coefficient matrix can be divided into four quadrants. The first quadrant contains the coefficients associated with Type I imperfections (γ_{2jk}), and the second quadrant contains Type II (γ_{1jk}) coefficients. The third and fourth sectors contain identity and zero matrices, respectively. Solving combined imperfection types yields a full coefficient matrix. All imperfections were considered individually and collectively.

Imperfection modes, N , describe the number of discretizations necessary to capture essential modal patterns in the imperfection field. For example, $N = 1$ implies one cosine wave in Type II imperfections, while $N = 64$ considers 64 individual cosine functions to

describe the actual imperfection pattern. Yeigh [1995] has shown that 128 imperfection modes were necessary to describe stochastic patterns. For the present study, *Figure 4.1* shows that only 64 modes are sufficient to provide an accurate description of imperfection patterns (input).

Buckling modes, M , are the eigenvector and provide the output, while imperfection patterns describe the input. For example, in the Euler column, the first mode is the dominant form. Depending on input parameters described as well as load configurations, higher-order modes can influence the eigenvalue problem significantly. Yeigh [1995] showed that for BEF, 16 modes were sufficient for convergence. In the present study, 16 modes were also sufficient for convergence (*Figure 4.2*).

The soil parameter, ϕ_0 , prescribes foundation stiffnesses where small numbers are describe soft foundations and large numbers describe firm foundations. A value of 225 represents moderate stiffness and is used in this study. The soil parameter significantly influences imperfection sensitivity. A reduction in ϕ_0 decreases imperfection sensitivity. This result is reasonable since $\phi_0 = 0$ is an Euler column, which is insensitive to imperfections (*Figure 4.3*). Based on earlier studies [Palassopoulos 1993, Yeigh 1995, Hoffman 1996], a ϕ_0 value of 225 is chosen for this study.

The classical buckling load, ρ_{cl} , refers to the applied load which causes the structure to buckle in the absence of imperfections. For actual structures the applied load, ρ , should be lower than the classical buckling load. Other researchers [Timoshenko and Gere 1961, Palassopoulos 1993, Yeigh 1995] have shown that the classical load for BEF is obtained by minimizing the expression of $(j^4 + \phi_0)/j^2$ where $j = 1, 2, 3, \dots, M$. The dominant buckling mode minimizes the corresponding classical load expression. In this study, 99, 97, 95, and 90% of the classical load were used to examine load factor effects.

As for all imperfections, temperature imperfections vary about their mean value, T_0 , described as the normalized average change in temperature. This normalization can be determined by dividing the mean change in temperature by the room temperature (which has been set at 30°C in this study). After analyzing the program output and considering its physical meaning, T_0 is set at -0.167, where a negative sign for T_0 means a reduction

in temperature. Temperature reduction is important because it introduces the internal compression load to the BEF, which increases the applied load. Furthermore, a reduction in T_0 causes an increase in the foundation stiffness. As mentioned before, an increase in the foundation stiffness causes an increase in imperfection sensitivity. A T_0 of 0.167 means a temperature change of 5°C from room temperature. This is a reasonable change in temperature for many real structures and especially for microelectromechanical systems (MEMS). The coefficient of thermal expansion, α , is a parameter that is used to define the amount of material expansion or contraction under temperature change, and has been normalized by the thermal expansion parameter for steel. In this study, steel is chosen because it is a material that is widely used; thus, α is set as 1.

A reduction in temperature causes an increase in foundation stiffness. The foundation stiffness factor, C_t , prescribes the percent increase in foundation stiffness when the temperature is reduced. C_t is normalized by the foundation stiffness, ϕ_0 , and is chosen to be -0.0024. This value represents about a 0.04% increase in foundation stiffness per degree decrease in temperature. After analyzing experimental results from Guyer and Brownell [1989] this is a reasonable value for steel members.

In this study, imperfection patterns are taken to be deterministic. In other words, the nature of imperfection patterns is known a priori. Although a specific functional form of imperfections is not required, a sine function is used for Type I (shape) imperfections and a cosine function is used for Type II (nonshape) imperfections. The use of a sine function is influenced by boundary conditions, where two ends of the beam must meet zero lateral displacement.

Different deterministic imperfection amplitude shapes have been tried to determine their relative importance. These imperfection amplitudes include shapes that are linearly increasing, constant, sine and cosine waves, square and square root functions. A cosine function is selected for all deterministic imperfection amplitude shapes because analysis has shown it is the most sensitive imperfection amplitude for all imperfections considered in this study. The magnitude of the imperfection is chosen as 0.002, but imperfection

magnitude does not affect the root mean square imperfection magnitude, ϵ_{RMS} . The RMS for imperfection magnitude $\epsilon_{RMS}^{(i)}$ can be solved from *Equations 4.1-4.5*:

$$\epsilon_{RMS}^{(i)t} = \epsilon_{cr}^{(i)} \sqrt{\frac{1}{\pi} \int_0^{\pi} [t^{(i)}(x)]^2 dx} \quad (4.1)$$

$$\epsilon_{RMS}^{(i)e} = \epsilon_{cr}^{(i)} \sqrt{\frac{1}{\pi} \int_0^{\pi} [e^{(i)}(x)]^2 dx} \quad (4.2)$$

$$\epsilon_{RMS}^{(i)k} = \epsilon_{cr}^{(i)} \sqrt{\frac{1}{\pi} \int_0^{\pi} [k^{(i)}(x)]^2 dx} \quad (4.3)$$

$$\epsilon_{RMS}^{(i)h} = \epsilon_{cr}^{(i)} \sqrt{\frac{1}{\pi} \int_0^{\pi} [h^{(i)}(x)]^2 dx} \quad (4.4)$$

$$\epsilon_{RMS}^{(i)f} = \epsilon_{cr}^{(i)} \sqrt{\frac{1}{\pi} \int_0^{\pi} [f^{(i)}(x)]^2 dx} \quad (4.5)$$

where $i = 1, 2, \dots, M$. The product of the imperfection magnitude ϵ_{cr} and RMS imperfection patterns should not be greater than 0.35 since it violates the nature of the perturbation approximation (Yeigh 1995). The imperfection amplitude shapes will affect the ϵ_{RMS} and not the imperfection magnitude.

Applied loads have been normalized by the classical (perfect) buckling load. All length variables have been normalized by the modified beam length, $L_p = L/\pi$ which help to ease evaluation of trigonometric functions (i.e. at 0 and π). Imperfection patterns $e(x)$, $f(x)$, $g(x)$, $h(x)$, and $t(x)$ represent variabilities in modulus of elasticity, foundation stiffness, moment of inertia, initial shape, and temperature.

In *Figures 4.4-4.9*, all ϵ_{RMS} have been truncated at 0.35, for which the power series does not converge with an ϵ_{RMS} greater than 0.35. Therefore, an ϵ_{RMS} value greater than 0.35 is physically meaningless.

From *Figure 4.4*, five imperfection patterns were analyzed individually and compared to assess the relative importance to each other. Shape appears to be the most

sensitive followed by temperature, foundation stiffness, moment of inertia, and modulus of elasticity. All Type II imperfections had ϵ_{RMS} similar in shape, orientation, and location. This result was anticipated since only γ_{1jk} in the potential energy was influenced by Type II imperfections.

A second observation from *Figure 4.4* is that BEF was determined to be the most sensitive to shape imperfections and the least sensitive to change in temperature imperfections (when the average change in temperature is -0.033°). The third observation is that the imperfection sensitivity for change in temperature imperfection increases when the magnitude increases of the mean value for change in temperature increases. This imperfection sensitivity can range from most sensitive to least sensitive in Type II imperfection.

In *Figure 4.5*, ϵ_{RMS} values for temperature are shown. The mean value for change in temperature is chosen as -0.167 to demonstrate its effects. This figure shows that $t(x)$ is the least sensitive by itself. The buckling strength of BEF is reduced when in the presence of other Type II imperfections. When all Type II imperfections are present together, ϵ_{RMS} can be reduced as much as 70%.

Figure 4.6 represents ρ/ρ_{cr} plotted as a function of ϵ^h_{RMS} and ϵ^t_{RMS} for temperature and shape imperfections. The purpose of these two figures is to determine additive effects of Type II imperfections on the existing temperature and shape imperfections. As shown in these two figures, there are no significant effects for the presence of other imperfections. All lines are essentially the same. This figure also shows that shape is the most dominant imperfection pattern.

Figures 4.7-4.9 represent ρ/ρ_{cr} plotted as a function of ϵ^c_{RMS} , ϵ^f_{RMS} , and ϵ^g_{RMS} . The presence of any Type II imperfections can reduce the ϵ_{RMS} , and the reduction can vary from 10 to 57%. The presence of Type I imperfections introduced a remarkable seventyfold increase in sensitivity.

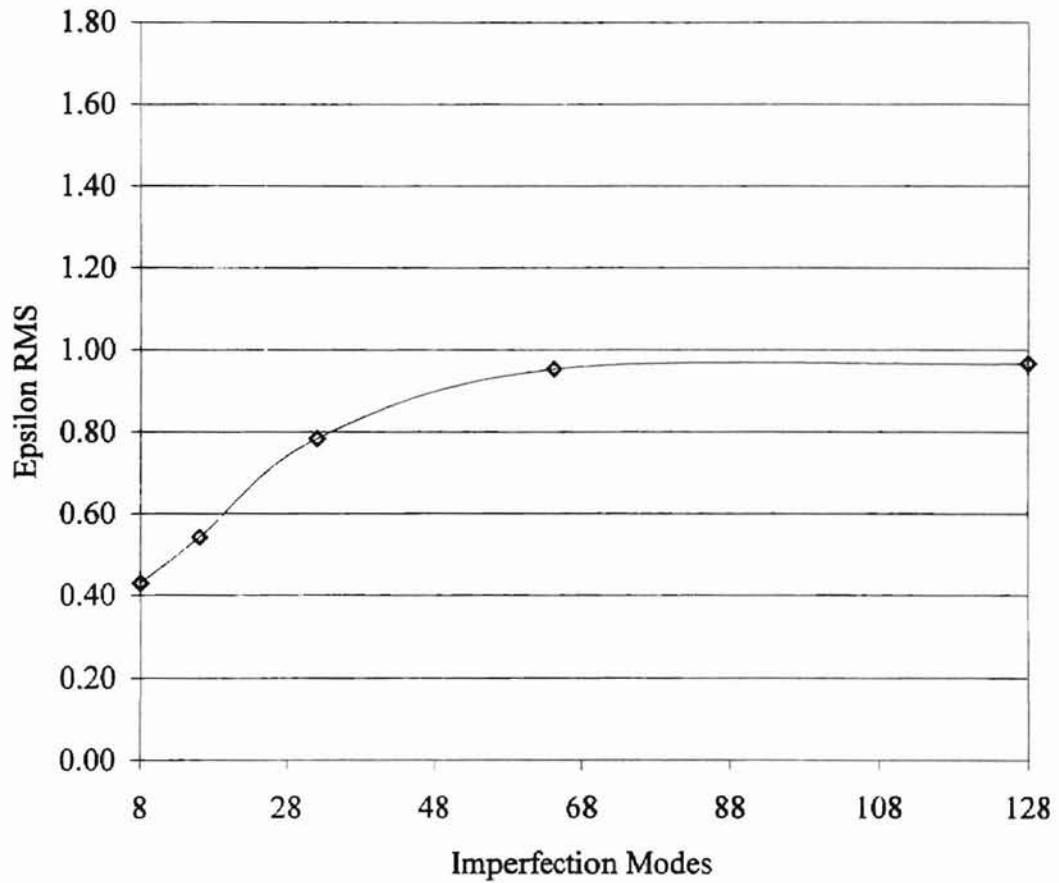


Figure 4.1. Convergence of Imperfection Modes

Foundation Stiffness, $\varphi_0 = 225$

Buckling Modes = 16

Normalized Average Change in Temperature = -0.167

Normalized Thermal Expansion Parameter = 1

Normalized Foundation Stiffness Factor = -0.0024

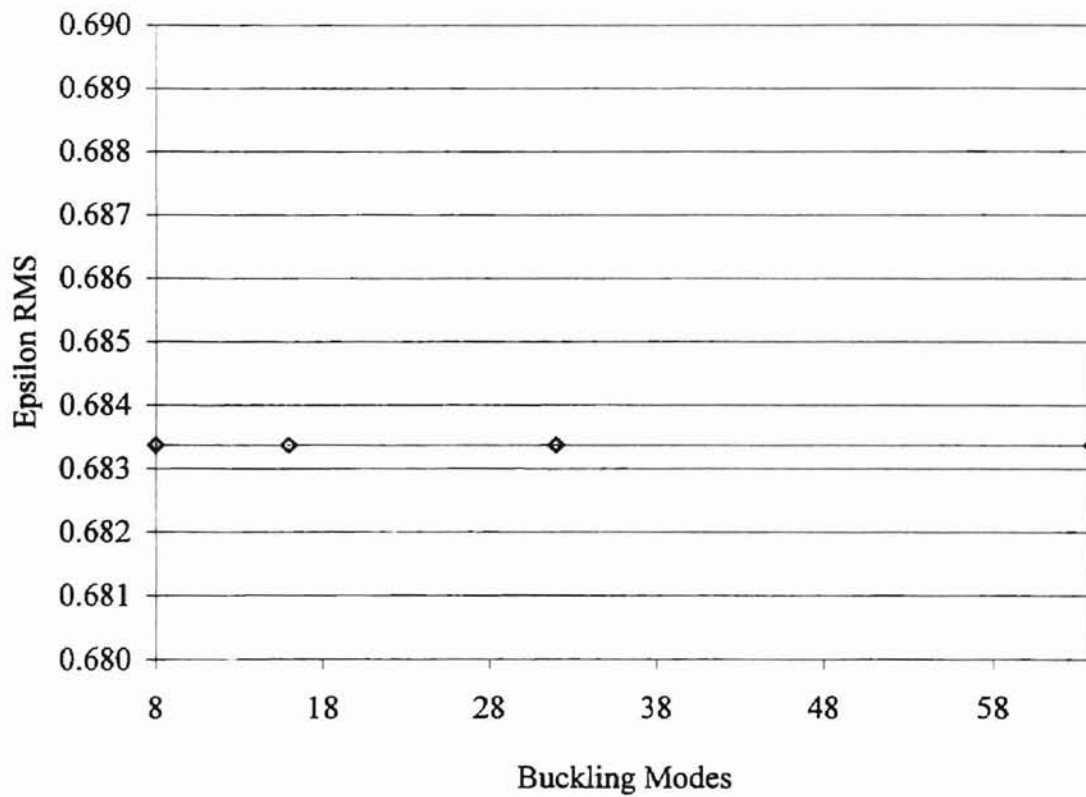


Figure 4.2. Convergence of Buckling Modes

Foundation Stiffness, $\varphi_0 = 225$

Imperfection Modes = 64

Normalized Average Change in Temperature = -0.167

Normalized Thermal Expansion Parameter = 1

Normalized Foundation Stiffness Factor = -0.0024

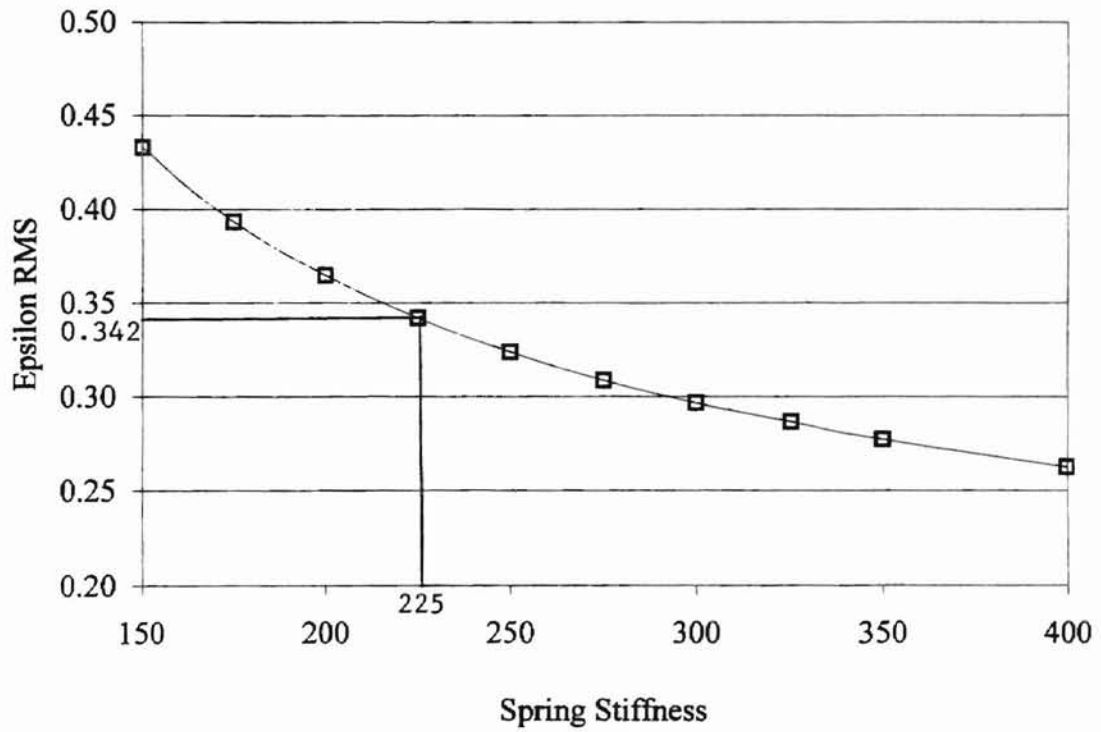


Figure 4.3. Effects of Foundation Stiffness on ϵ_{RMS}^f

Imperfection Modes = 64

Buckling Modes = 16

Dimensionless Load Ratio = 99%

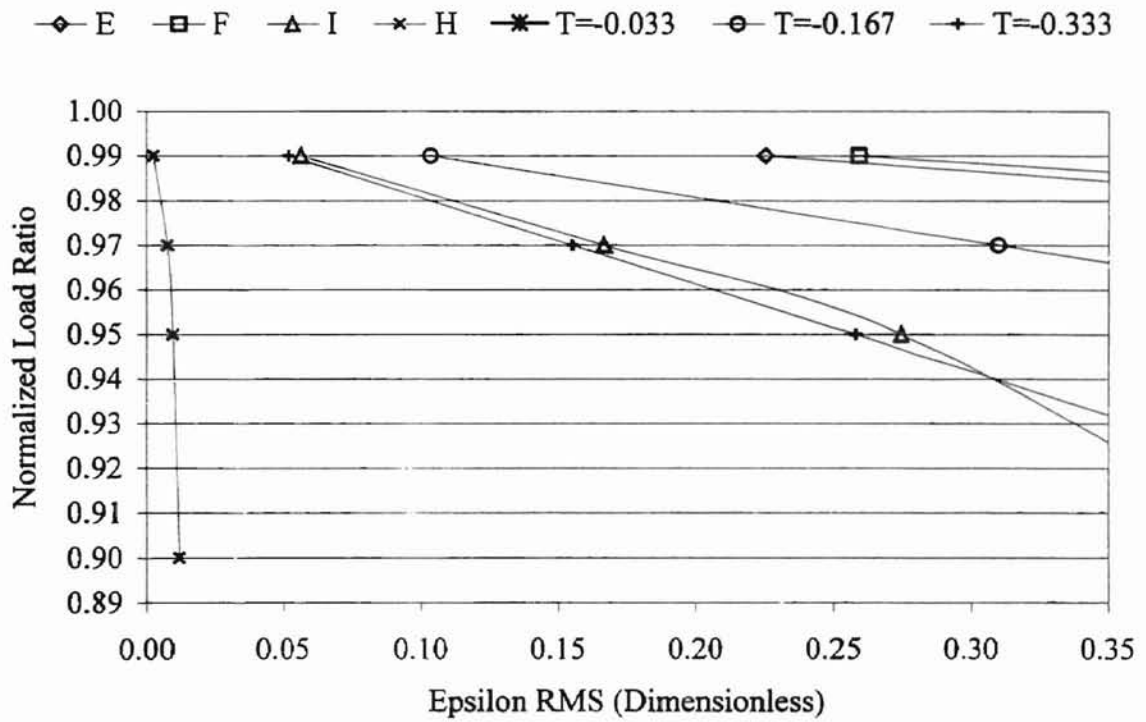


Figure 4.4. Direct Comparison of e, f, g, h, and t

Foundation Stiffness, $\varphi_0 = 225$

Imperfection Modes = 64

Buckling Modes = 16

Normalized Thermal Expansion Parameter = 1

Normalized Foundation Stiffness Factor = -0.0024

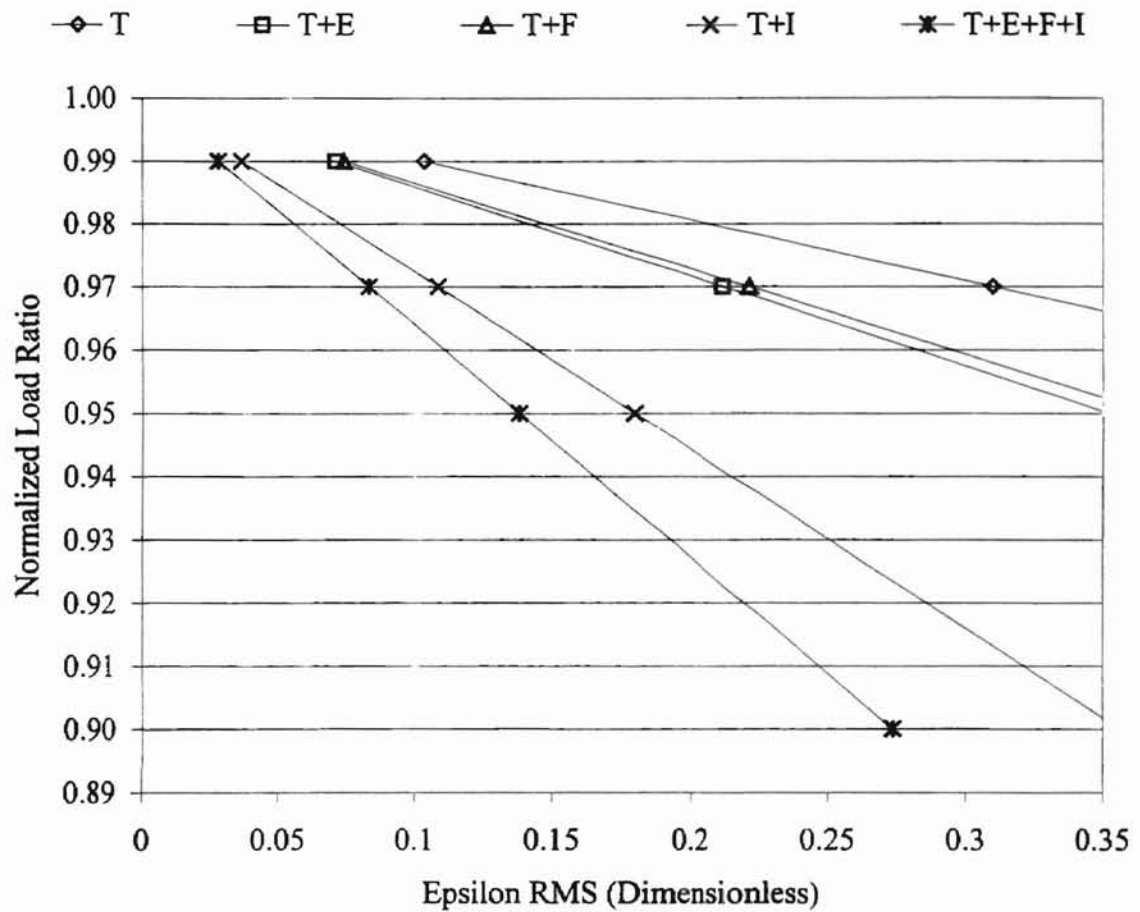


Figure 4.5. Effects on Change in Temperature ϵ_{RMS}^I

Foundation Stiffness, $\varphi_0 = 225$

Imperfection Modes = 64

Buckling Modes = 16

Normalized Average Change in Temperature = -0.167

Normalized Thermal Expansion Parameter = 1

Normalized Foundation Stiffness Factor = -0.0024

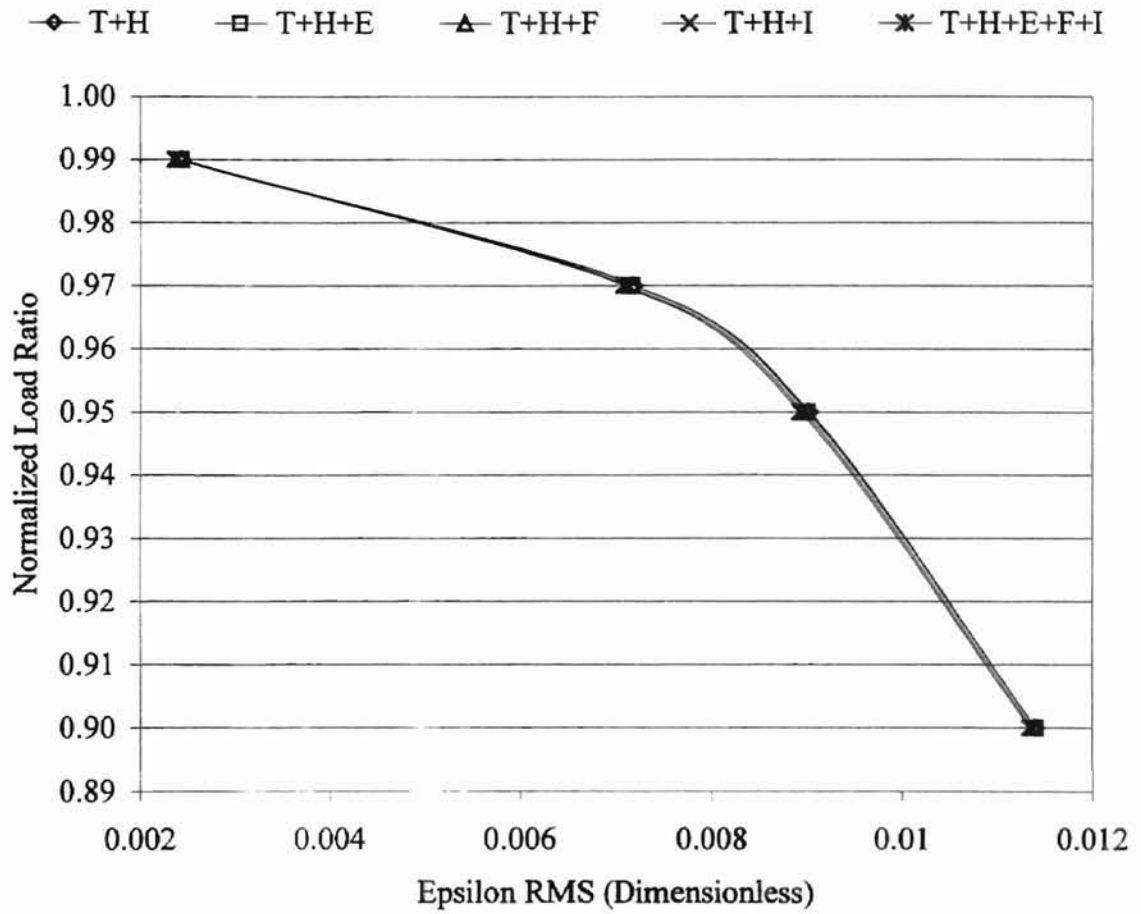


Figure 4.6. Effects on Initial Shape and Temperature ϵ^h_{RMS} and ϵ^l_{RMS}

Foundation Stiffness, $\varphi_0 = 225$

Imperfection Modes = 64

Buckling Modes = 16

Normalized Average Change in Temperature = -0.167

Normalized Thermal Expansion Parameter = 1

Normalized Foundation Stiffness Factor = -0.0024

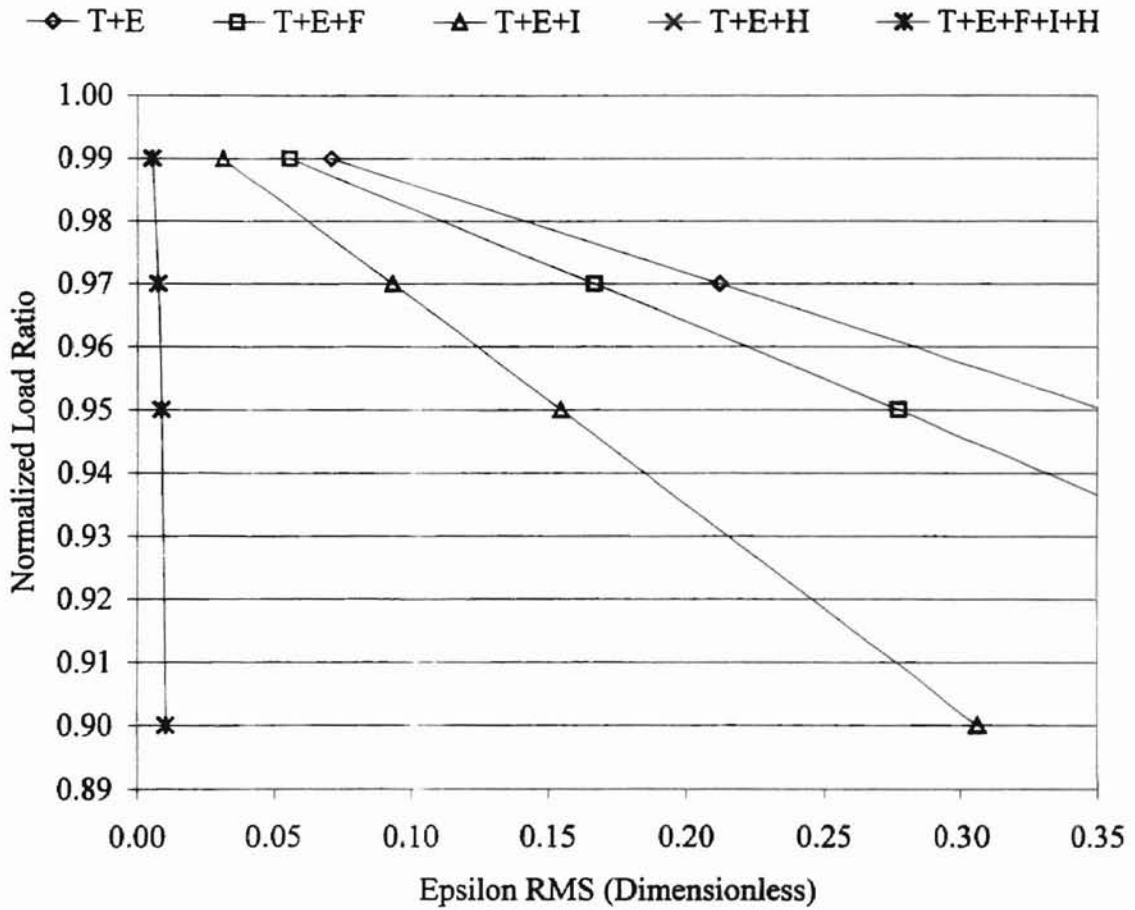


Figure 4.7. Effects on Modulus of Elasticity ϵ_{RMS}^c

Foundation Stiffness, $\varphi_0 = 225$

Imperfection Modes = 64

Buckling Modes = 16

Normalized Average Change in Temperature = -0.167

Normalized Thermal Expansion Parameter = 1

Normalized Foundation Stiffness Factor = -0.0024

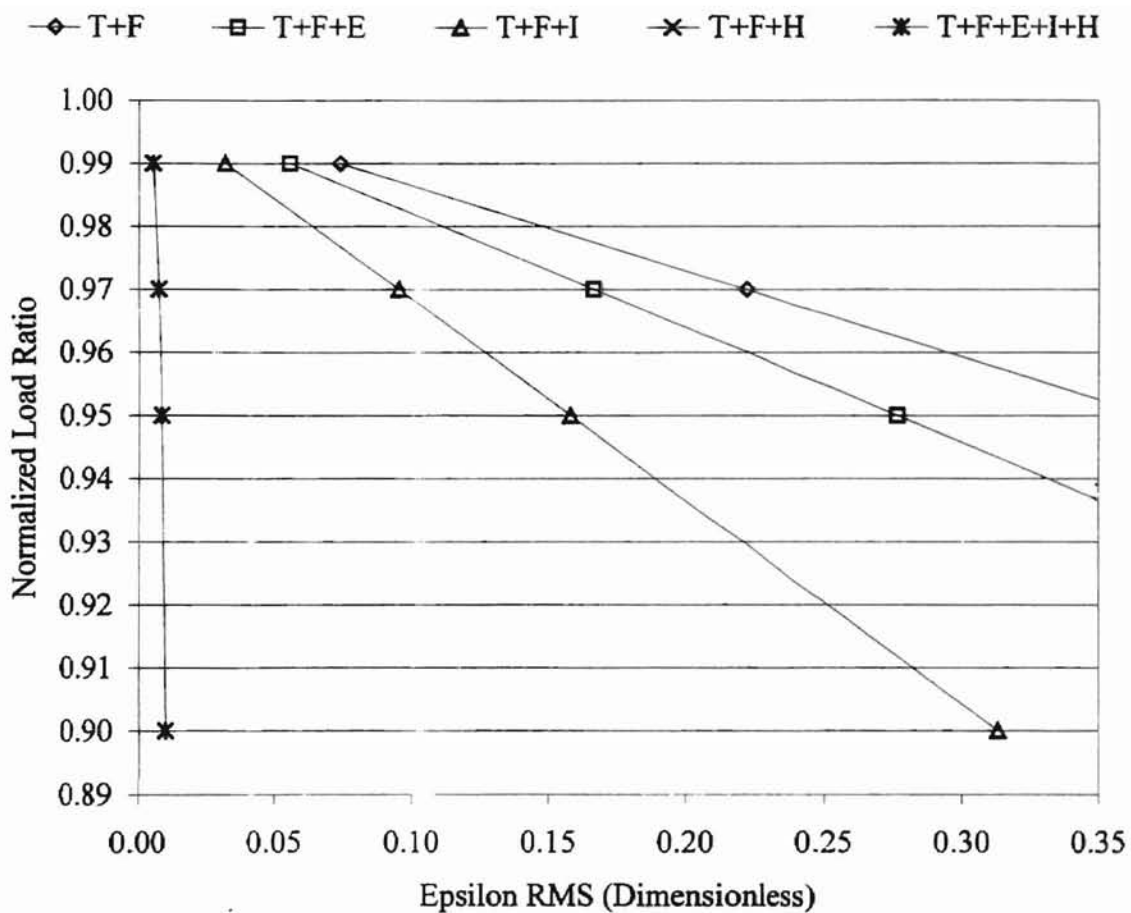


Figure 4.8. Effects on Foundation Stiffness ϵ_{RMS}^f

Foundation Stiffness, $\varphi_0 = 225$

Imperfection Modes = 64

Buckling Modes = 16

Normalized Average Change in Temperature = -0.167

Normalized Thermal Expansion Parameter = 1

Normalized Foundation Stiffness Factor = -0.0024

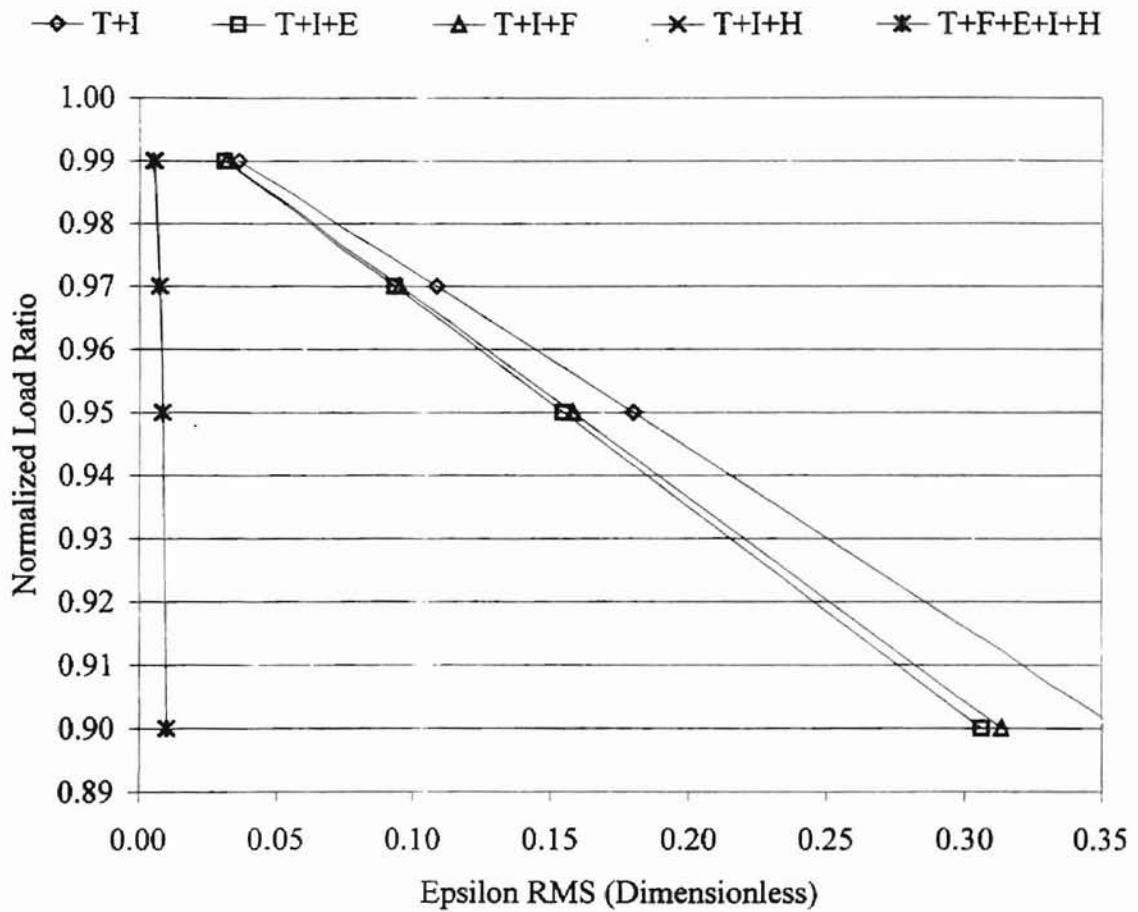


Figure 4.9. Effects on Moment of Inertia ϵ_{RMS}^i

Foundation Stiffness, $\phi_0 = 225$

Imperfection Modes = 64

Buckling Modes = 16

Normalized Average Change in Temperature = -0.167

Normalized Thermal Expansion Parameter = 1

Normalized Foundation Stiffness Factor = -0.0024

CHAPTER 5

CONCLUSIONS

Today, everything has been pushed to its extreme limits. Mechanical devices have been miniaturized to micro/nano-scale levels. Metal sheetwalls of a building can be as thin as a few millimeters while maintaining its strength. Therefore, imperfections have become increasingly vital in stability analysis. This study has considered imperfection effects on a beam on elastic foundation (BEF). The critical imperfection magnitude method has been used to analyze the significance of imperfections and their imperfection interactions on BEF.

Small, uncontrolled deviations in temperature from the mean value, T_0 , have a negligible effect on the stability of BEF. In fact, temperature has the least impact when normalized average change in temperature is less than -0.033. If the mean value or amplitude of imperfections is large, temperature imperfections can have adverse effects. Normalized average change in temperature of -0.4, -0.233, -0.167, and -0.067 will reduce the effective buckling load to 90, 95, 97, and 99% of the classical value.

Even though the effects of temperature imperfection alone are insignificant, thermal imperfections can stimulate other material and geometric imperfections. When foundation stiffness imperfections are coupled with -0.167 variability in temperature, the load factor could be reduced to 71% of the classical value. Thermal imperfections behave in the same manner as other Type II imperfections, while shape imperfections appear to be most sensitive to BEF. When thermal and shape imperfections were combined, all other imperfections were shown to have diminished effects.

The critical imperfection magnitude method used in this study was strongly influenced by shape imperfection patterns. If all imperfection patterns for real structures

are known, this deterministic study can be used to accurately determine the effects of those imperfections. If imperfection patterns are not known, stochastic methods can be used to accurately simulate imperfection patterns [Yeigh 1995, Hoffman 1996].

REFERENCES

- Almroth, B.O., A.M.C. Holmes, and D.O. Brush. "An Experimental Study of the Buckling of Cylinders Under Axial Compression." *Experimental Mechanics* (September 1964), pp. 263-270.
- Bazant, Z. and L. Cedolin. *Stability of Structures*, Oxford, 1991.
- Guyer, E.C. and D.L. Brownell. *Handbook of Applied Thermal Design*. New York: McGraw Hill, 1989.
- Hoffman, J.A. "Stability of Structures Subjected to Eccentric Load Imperfections." M.S. thesis, Oklahoma State University, 1996.
- Koiter, W.T. "On the Stability of Elastic Equilibrium." Ph.D. thesis. Delft, Holland, 1967.
- Langhaar, H.L. *Energy Method in Applied Mechanics*. Melbourne: Krieger, 1989.
- Palassopoulos, G.V. "A New approach to the Buckling of Imperfection-Sensitive Structures." *Journal of Engineering Mechanics*, Vol. 119, No. 4, (April 1993), pp. 850-869.
- Palassopoulos, G.V. "Response Variability of Structures Subjected to Bifurcation Buckling." *Journal of Engineering Mechanics*, Vol. 118, No.6, (June 1992), pp. 1164-1183.
- Simitses, G.J. *An Introduction to the Elastic Stability of Structures*. Melbourne: Krieger, 1976.
- Tennyson, R.C., D.B. Muggerridge, and R.D. Caswell. "Buckling of Cylindrical Shells Having Axisymmetric Imperfection Distributions." *AIAA Journal*, Vol. 9, No. 5, (1971), pp. 924-930.
- Thompson, J.M.T. and G.W. Hunt. *Elastic Instability Phenomena*. New York: Wiley, 1984.
- Timoshenko, S.P. and J.M. Gere. *Theory of Elastic Stability*. New York: McGraw-Hill, 1961.
- Yeigh, B.W. "Imperfections and Instabilities." Ph.D. thesis, Princeton University, 1995.

VITA

Kah-Kan Chan

Candidate for the Degree of

Master of Science

Thesis: STABILITY OF BEAMS SUBJECTED TO THERMAL IMPERFECTIONS

Major Field: Civil Engineering

Biographical:

Personal Data: Born in Ipoh, Perak, Malaysia, on September 7, 1975, the son of Hock-Seng Chan and Swee-Kam Lee.

Education: Graduated from Poi Lam High School, Ipoh, Parak, Malaysia, in December, 1993; received the Bachelor of Science degree in Civil Engineering from Oklahoma State University, Stillwater, Oklahoma, in December, 1997; completed requirements for the Master of Science degree with a major in Civil Engineering at Oklahoma State University in July, 1999.

Experience: Undergraduate grader and graduate research assistant for the School of Civil and Environmental Engineering, Oklahoma State University, 1998 to present.

Professional Memberships: American Society of Civil Engineers, Chi Epsilon, Tau Beta Pi, and Phi Kappa Phi honor societies.